AGU
ADVANCING EARTH AND SPACE SCIENCE

Geophysical Research Letters®

Key Points:

- The size distribution and numerical density of salt particles formed from sublimating salty ices were quantified for the first time
- Micrometer-sized particles arise from low salinity ices (<3.5 psu) below −30 °C; in 0.085 psu ices, they form at any subzero temperature
- >100 μm particles are produced by sublimation above −21 °C in ices above 0.85 psu, and at any temperature in those exceeding 35 psu

Temperature and Concentration Affect Particle Size Upon Sublimation of Saline Ice: Implications for Sea Salt Aerosol Production in Polar Regions

Kamila Závacká[1], Vilém Neděla[1] , Martin Olbert[1] , Eva Tihlaříková[1] , Ľubica Vetráková[1] , Xin Yang[2] , and Dominik Heger[3]

[1]Environmental Electron Microscopy Group, Institute of Scientific Instruments of the Czech Academy of Sciences, Brno, Czech Republic, [2]British Antarctic Survey, Natural Environment Research Council, Cambridge, UK, [3]Department of Chemistry, Masaryk University, Brno, Czech Republic

Abstract Using an environmental scanning electron microscope, we quantified for the first time aerosol-sized salt particles formed during the sublimation of sea ice as a function of temperature and concentration. The sublimation temperature of the ice is a dominating physical factor to determine the size of the residua: Below −20°C, micron-sized pieces of salt emerge, whereas above the temperature large chunks of salt are detected. Another such aspect influencing the distribution of sizes in salt particles is the concentration: Micron-sized particles are observed exclusively at salinities below 3.5 psu, while below 0.085 psu particles with a median smaller than 6 μm arise from sea ices at any subzero temperature. Moreover, when a chunk of salt sublimes at less than −30°C to be dried and warmed later, a large number of sub-micron crystals will appear. We relate our findings to the production of the polar atmospheric sea salt aerosols.

Plain Language Summary In polar regions, saline ices on sea ice or at coastal areas are thought to be a direct source of chemical compounds and sea salt aerosols; these salty aerosols are important to polar atmospheric chemistry and global climate for various reasons, such as that they affect atmospheric radiation in both a direct and an indirect manner. However, the exact location of the salts within the ice, together with the temperature and concentration dependence of the size and number density of the salt particles formed, was previously poorly understood and not well quantified. We therefore utilized a unique electron microscope to observe the structural changes occurring when saline ices sublime to create salt particles. Our experiments showed that small salt particles, proxies of sea salt aerosols, are preferably generated from low-concentrated ices and at low temperatures. These microscopic observations provide direct laboratory evidence to the proposed mechanism of sea salt aerosol production from sublimating saline ice and snow and may help us to fit the missing piece of information into the puzzle of polar spring ozone depletion and bromine explosion events.

1. Introduction

Sea salt aerosols (SSAs) strongly influence regional climates via their role as cloud condensation nuclei (O'Dowd et al., 1997) and ice-nucleating particles (DeMott et al., 2016; Wise et al., 2012), thus impacting on radiative forcing (Murphy et al., 1998; Murray et al., 2021; Neubauer et al., 2019). In addition, SSAs are of great importance in atmospheric chemistry due to their submicron and micron-sized structures and large quantities, offering an immense specific surface area for heterogeneous chemical reactions (Bertram et al., 2018; Wilson et al., 2015; Yang et al., 2019). In polar regions, SSAs, together with salty ice surfaces, are assumed to be the key media in bromine explosion events (BEEs), which usually associate with ozone depletion events (ODEs) (Keiichiro Hara et al., 2018; Shepson, 2021). Such occurrences are characterized by surface ozone level concentrations below 10 ppbv (part per billion volume); the typical background values range between 30 and 40 ppbv (Barrie et al., 1988; Tarasick & Bottenheim, 2002). Over the open ocean, SSAs originate from bubble bursting and wave breaking (Keene et al., 2007); however, they can be also produced in open leads (Kirpes et al., 2019; Leck et al., 2002; May et al., 2016; Nilsson et al., 2001). In addition, SSAs were proposed to be based on frozen salty solutions, such as those embodied in sea ice, sea-water contaminated snow, frost flowers (FFs) (Kaleschke, 2004), and blowing snow (Yang et al., 2008). The extent of the sources' relative contributions and their intensification at particular conditions have not been defined to date (Abbatt et al., 2012). The fact that sea ice zones are a large source of SSAs was deduced from the sulfate depletion relative to sodium in SSAs and snow with respect to sea

Writing – original draft: Kamila Závacká, Martin Olbert, Ľubica Vetráková, Dominik Heger
Writing – review & editing: Xin Yang, Dominik Heger

water in coastal regions and inland Antarctica (K. Hara et al., 2004; Wagenbach et al., 1998). The global models show that the observed winter peak of sodium in SSAs in polar regions cannot be produced solely by sea spray from open water, due to the longer distances from the open ocean in winter; however, when sea ice-sourced SSAs are implemented, the winter peak can be reproduced well (Rhodes et al., 2017; Yang et al., 2019). Until now, the role and effect of the newly identified blowing snow-induced production of SSAs in polar climate and atmospheric chemistry have not been sufficiently explored and remain rather obscure.

Previously, the microscopic observation focused on the ice with impurities or the aerosols; by contrast, to the best of our knowledge, no detailed report on the sea ice sublimation process and the resulting particles has been proposed thus far. Investigations utilizing the low temperature scanning electron microscope (SEM) revealed that dissolved impurities can be present in the grain boundaries, the veins (triple junctions) of metamorphosed snow (Chen & Baker, 2010; Domine et al., 2003), and polar glaciers (Barnes et al., 2002; Cullen & Baker, 2001; Mulvaney et al., 1988). Micrometric inclusions and crystals were identified with either X-ray dispersion or Raman analysis (Ohno et al., 2005; Sakurai et al., 2009). Sublimating the ice, that is, sintering, found use as a method to increase the concentration of impurities in polar ice cores (Oyabu et al., 2020); exhaustive sublimation then yielded an ice grain cast (Rosenthal et al., 2007). Optical microscopy was applied in the observation of gaseous and solid inclusions in natural ices at temperatures above −25°C (Killawee et al., 1998; Light et al., 2003). Analyzing sea spray aerosols from open sea ice leads exposed a large contribution of marine organic compounds, in addition to that of the sea salts (Kirpes et al., 2019); the native conditions of the compounds were studied via cryo-TEM (Patterson et al., 2016). Impurity inclusions in laboratory-made ices were monitored in NaCl (Blackford et al., 2007; Light et al., 2009; Yang et al., 2017), CsCl, and rose bengal (Hullar & Anastasio, 2016; Vetráková et al., 2019), showing a strong influence of the sample preparation. The sublimation of frozen aerosols containing organics in an environmental chamber showed that the aerosols can become very porose to expand from their original volumes (Adler et al., 2013); an analogy to atmospheric freeze-drying in ice clouds is inferable.

The role of the temperature in both the occurrence of bromine explosion events (BEEs) and ozone depletion events (ODEs) in polar spring and the production of SSAs from saline substances has not been unambiguously characterized thus far. Previous in situ data showed that most of the ozone depletion events (ODEs) were observed at temperatures below −20°C (Tarasick & Bottenheim, 2002), despite some exceptions at higher temperatures (Bottenheim et al., 2009). As regards the relationship between BrO radicals and increasing temperature (in the range of −24 to −15°C), a close-to-linear decrease was revealed under solar radiation (Pohler et al., 2010). Similarly, in BrO, a linear decrease with increasing temperature was observed up to 0°C (Bognar et al., 2020). An other study, however, did not recognize the local temperature as an important factor (Halfacre et al., 2014). Apparently, the atmospheric observations do not link the ODEs and bromine explosion events (BEEs) with the temperature in a straightforward manner (Bognar et al., 2020).

The genesis of SSA production from blowing snow on sea ice is assumed to be proportional to the snow salinity and sublimation flux of the blowing snow, which is a complex function of the wind speed, temperature, and humidity (Yang et al., 2008, 2019). Although the threshold wind speed for the blowing snow was found to depend on the air temperature (Li & Pomeroy, 1997), the proposed SSA formation mechanism itself does not indicate a temperature-dependent relationship. SSAs were previously also considered to directly arise from FFs (Rankin, 2002); recent laboratory research nevertheless provided evidence that, at temperatures above the eutectic point of NaCl solutions (−21.2°C) (Brady, 2009), FFs cannot produce micron-sized SSAs (Roscoe et al., 2011; Yang et al., 2017). The role of temperatures below the eutectic point of NaCl has not been defined yet. Thus, in this study we undertake microscopic examination of sublimating sea ices at various temperatures and salt concentrations to explore the microscopic-level processes, and we also discuss the implications for polar SSAs.

2. Materials and Methods

2.1. Environmental Scanning Electron Microscope (ESEM)

The microscopic images were recorded with an ESEM AQUASEM II redesigned from a Tescan SEM VEGA (Nedela, 2007); the microscope comprised a Peltier-cooled sample holder. The electron beam energy of 20 keV and a current of 100 pA were applied to scan the sample, with the backscattered electrons detected by a YAG:Ce^{3+} scintillation detector (Neděla et al., 2018). To acquire the high-resolution images and to perform the

energy dispersive spectroscopy (EDS), we employed an ESEM Quanta 650 FEG at +20°C, after thorough water sublimation (see the detailed description in Text S1 of Supporting Information S1) (Neděla et al., 2015). The resolution is ~400 nm, limiting our observation of fine particles.

2.2. Freezing and Sublimation

Sea salt solutions with the salinities of 0.085, 0.85, 3.5, 35, and 78 psu were prepared by dissolving an appropriate amount of synthetic sea salt (Sigma S9883) in demineralized water. A droplet (5 μl) of the solution was placed onto a silicon pad on the Peltier cooling stage of the ESEM and then cooled down to one of the final sublimation temperatures, that is, −16, −30, or −40°C. Regarding the Peltier stage (see Text S2 in Supporting Information S1 for the calibration), the temperature progress in time is shown in Figure S1 of Supporting Information S1. The freezing occurred spontaneously, and its temperature was determined with a thermocouple to range between −10 and −14°C. The frozen samples were sublimed after controlled evacuation of the ESEM specimen chamber at a nitrogen pressure of between 10 and 300 Pa.

3. Results

The sublimation of ice from a frozen sample yielded sea salt particles and crystals with a reproducible morphology for each combination of a concentration and a sublimation temperature. The main features and the particle shape statistics are presented in Figure 1 and Table S1 of Supporting Information S1, respectively. As the lowest examined concentration (0.085 psu) produced solely separate particles, these clearly appear in white on a black silicon pad (for the original images, see Figure S2 in Supporting Information S1); the particles were counted and examined in terms of their maximum dimensions (d) and aspect ratio (Text S3 in Supporting Information S1, Figure S3 in Supporting Information S1). All the other micrographs are displayed in the original gray shades, which reveal particles, crystals, and filaments attached to the silicon pad. The particle analysis was also possible for the 0.85 and 3.5 psu concentrations sublimed at −30 and −40°C. Under the other conditions, the salt interconnected into large clusters. Generally, the edges of the original drop were characterized by amounts of particles lower than those in the centers. The crowding in the central part of the drop can be explained by (a) a greater height of the drop and (b) the drag of the particles during the sublimation. The nonparametric Mann-Whitney-Wilcoxon statistical tests were employed to determine the difference between the particle population sizes.

3.1. Sublimating the 0.085 psu Ice

At the lowest examined concentration of 0.085 psu, the sublimation yielded tiny salt particles (Figure 1), whose maximum length and appearance were found to depend on the sublimation temperature (Figure S3a in Supporting Information S1). The diameters of the particles formed through sublimation at −16°C (median = 4.5, interquartile range (IQR) = 3.4–6.1, mean = 5.2 μm) are, on average, slightly smaller than those of the particles sublimed at −40°C (median = 5.7, interquartile range (IQR) = 3.7–9.7, mean = 7.7 μm). This subtle difference can be rationalized via the shape analyses (see Text S4 in Supporting Information S1).

3.2. Sublimating the ≥0.85 psu Ice at −16°C

The sublimation residua at −16°C and −20°C (the latter are not shown) in all of the higher concentrations, that is, 0.85–78 psu, have common characteristics and will therefore be described together in this paragraph. As most of the salts composing the sea water are at these temperatures, the liquid solution evaporates concurrently with the ice sublimation. Thus, planar salt crystals attached to the silicon pad are always visible. The original concentration dictates the sizes of the resulting salt crystals. In 0.85 psu, for example, the image in Figure 1 displays the boundary between the original separate droplets (left lower sector); such a layout then results in a number of smaller crystals (median = 6.49, interquartile range [IQR] = 4.48–9.44, mean = 7.13 μm) and one larger drop (in the center), from which there arise concentrically grown crystals. The varied shapes of the crystals are likely to be indicative of distinct minerals, as exemplified via the EDS spectroscopy in Figure S10 of Supporting Information S1. The shapes resemble those of the efflorescence-produced crystals, (Patterson et al., 2016) indicating that
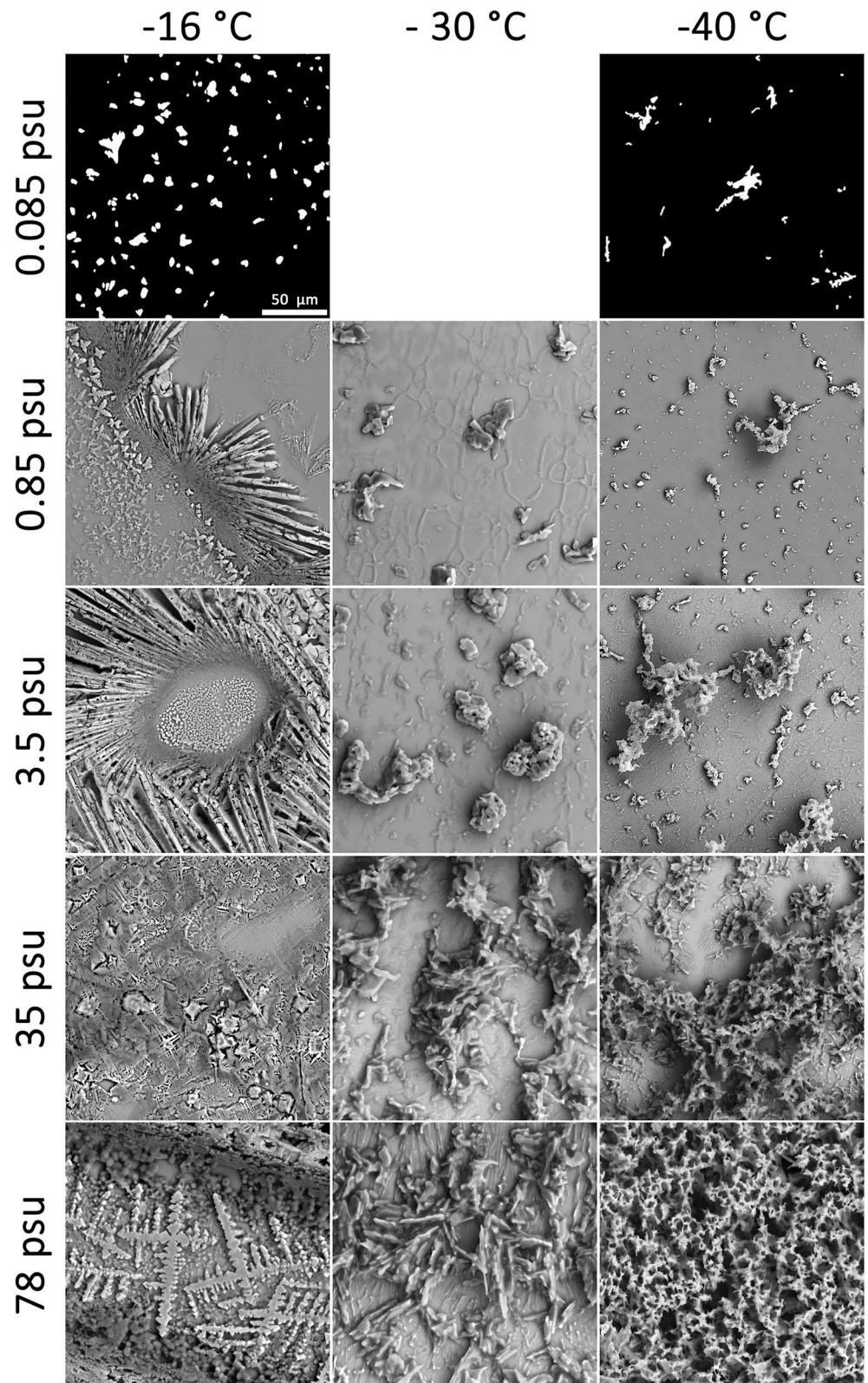
Figure 1. The structure of the sea salt residua after the sublimation of the 0.085, 0.85, 3.5, 35, and 78 psu frozen samples at −16, −30, and −40°C. The micrographs relating to 0.085 psu were contrasted; the scale in the first image applies to all others.
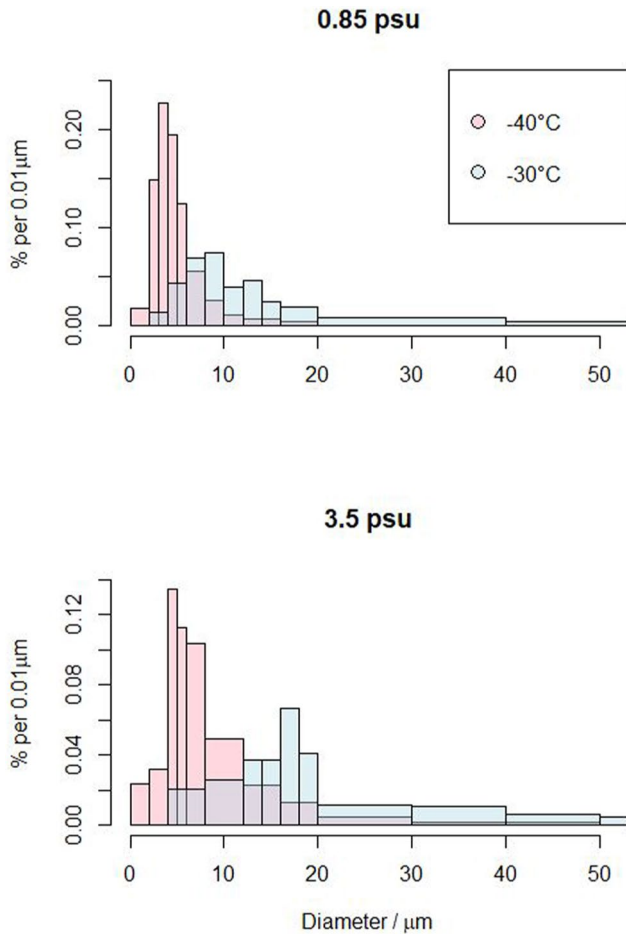
Figure 2. The histograms showing the distribution of the largest particle diameters after the sea ice sublimation at −40°C (red) and −30°C (blue) as a function of salinity; the smallest applied interval is 1 μm. The data are truncated at 51 μm (see Table S1 in Supporting Information S1 and Figures S6 and S7 in Supporting Information S1 for the full datasets); the instrumental resolution equals 400 nm.

both types of crystals share the same genesis. At concentrations higher than 35 psu, the silicon pad is fully covered with salt crystals of various geometrical shapes (dendritic structures, stars, rectangles). In one particular case, we observed the fractional crystallization of NaCl and $CaSO_4$ (Figure S11 in Supporting Information S1) by using EDS spectroscopy. The synoptical micrographs having the lowest resolution revealed the evolution of the crystallization patterns during the evaporation (Figure S4 in Supporting Information S1). The crystal morphology patterns take the form of concentric circles.

3.3. Sublimating the ≥0.85 psu Ice at −30 and −40°C

In the residua obtained through the sublimation at −30 and −40°C, we observed that the particle sizes increase with rising concentration and temperature (Figure 2). The concentration dependence can be clearly demonstrated on the sublimation of the 0.85 and 3.5 psu samples at −40°C (Figure S5 in Supporting Information S1): Most probably, at this concentration range and with the applied freezing method the veins and walls surrounding the ice crystals are not fully wetted with the brine, and this is even less so at the lower concentrations, resulting in smaller particles. Our analyses of the micrographs are summarized by the medians, IQRs, and means, the values being 4.4, 3.4–6.3, and 6.6 μm at 0.85 psu and 7.3, 5.1–11.6, and 11.2 μm at 3.5 psu. Above 3.5 psu, the brine sublimes into large clusters, which prevent their diameters from being analyzed. Nevertheless, optical inspections of the micrographs show that at 35 psu the image is not entirely filled with salt clusters, unlike the situation at 78 psu (excluding the edges of the sample). At this highest examined concentration, regular structures of salt aggregates are observed, which can be considered indicative of fully wetted veins between the ice crystals. The sublimation residua often assume sponge-like structures.

The role of the temperature in the sublimation is apparent from both the micrographs and the statistics that describe them (Figure 1, Figures S6 and S7 in Supporting Information S1). The crystals formed at −30°C do not exhibit features as sharp as those formed at −40°C; this is true of all the concentrations but becomes more discernible at the higher ones. The particle diameter distributions at 0.85 and 3.5 psu show a notable increase in the sublimation at −30°C as compared to the process at −40°C (Figure 2, Figures S6 and S7 in Supporting Information S1). Especially notable is the diminishing of particles whose diameters range below 10 μm: Apparently, a minority of salts liquid at −30°C suffices to conjoin smaller particles into larger ones in the sublimation process. A similar conclusion can be drawn from observing the residual salt filaments, as described in Text S5 and Figure S8 of Supporting Information S1.

3.4. Drying and Warming to +20°C

Lastly, the sublimation residua were further dried, and their temperature increased to +20°C. These processes then resulted in a very large number of small crystals; more concretely, in the sublimation residua of sea ice having 35 psu and sublimed at −40°C a full 75% of the crystals exhibited a side dimension below one micrometer (Figure 3, Figure S9 in Supporting Information S1; range = 0.4–2.5 μm, IQR = 0.63–0.94 μm). A similar trend was observed in the sublimation residua formed at −30°C (not shown), as opposed to those emerging at −16°C, which possessed solid monolithic salt structures (Figures S10, S11 in Supporting Information S1). Furthermore, an elemental analysis of the sublimation residua was performed, finding areas of Na and Cl excluded from Mg, Ca, K, S, and O to identify fractional salt crystallization of $MgSO_4$, $CaSO_4$, and, possibly, other sulfates (Figure S12 in Supporting Information S1).
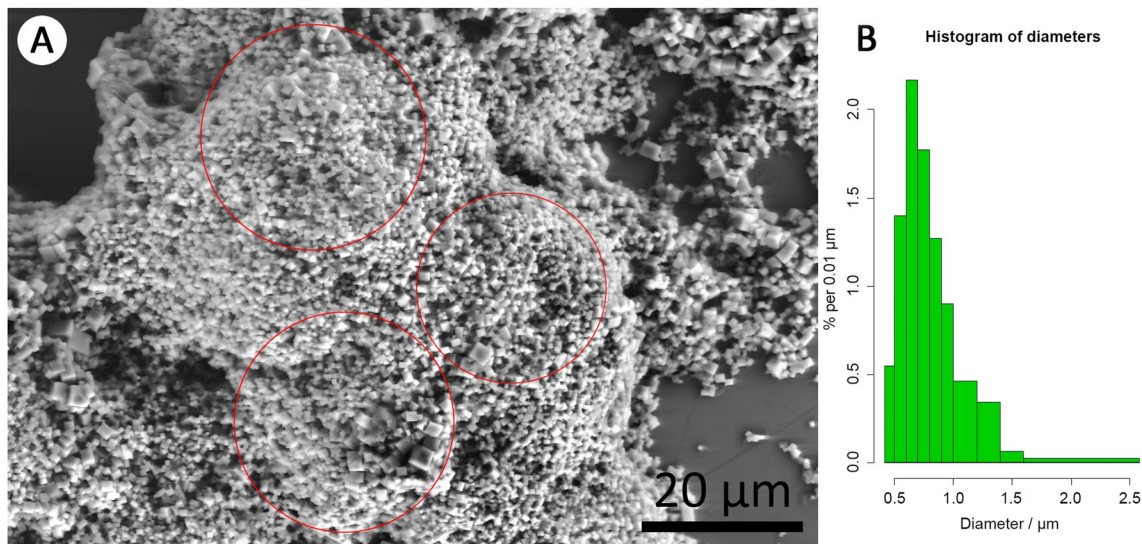
Figure 3. A micrograph of the 35 psu sea salt sublimed at −40°C and subsequently warmed to +20°C, (a) Encircled are the analyzed areas, whose particle size distribution is shown in the histogram, (b).

4. Discussion and Implications for the Formation of SSAs

The central item of knowledge obtained through the microscopic observations is a strong dependence of the amount and size of the salt crystals on both the ice sublimation temperature and the concentration of the original solution. At all but the lowest concentrations examined (0.085 psu), the sublimation above the NaCl's eutectic temperature (T_e) resulted in large pieces of salt, whose sizes often exceeded 100 micrometers (Figure 1). Such large particles have a very short airborne lifetime because they will soon be deposited back onto the ground due to the gravity sedimentation, even if carried by the wind; thus, they cannot act as SSAs. The formation of these large salt crystals at temperatures above −20°C embodies a consequence of the brine, which is mostly liquid inside the ice matrix (Light et al., 2003; Yang et al., 2017); as the ice sublimes, the liquid brine from the channels surfaces, accumulates at the edge of the sample, and crystallizes, producing large chunks of salt. This finding establishes a temperature bound of −20°C, above which SSAs will likely not form at the early stage of sea ice formation unless the concentrated brine has been diluted to very low levels of <0.085 psu. Conversely, at low temperatures (below −30°C), less liquid brine is present, and the sublimation process thus yields micrometer-sized particles (IQRs: 3.4–6.3 μm in 0.85 psu and 5.1–11.6 μm in 3.5 psu), given concentrations below 3.5 psu. Such an observation can be rationalized by assuming that the veins (triple junctions) and cell walls around the individual ice crystals contain the brine (Vetráková et al., 2020); the diameter of the veins, typically 2.5 micrometers (Vetráková et al., 2019), defines the particle dimension. Below the T_e of the individual salts, the brine partly solidifies via fractional crystallization (Figures S10–S12 in Supporting Information S1), reduces its flow, and breaks into small pieces (Figure 1). The fact that the particles are larger upon sublimation at −30°C than at −40°C (Figure 2) can be explained by the overall T_e of sea salt, whose value is supposed to reach −36.2°C according to the Gitterman pathway of salt precipitation (Marion et al., 1999). The occurrence of micrometric salt particles at the lowest examined concentration (0.085 psu), with the ice subliming at any subzero temperature, is simply a consequence of brine separation by the ice matrix. Thus, SSAs are expected to arise from sea ices of comparably low salinities at any subzero temperature. The observation can be extrapolated to a salinity lower than that of our experiments, where fine aerosol particles having a long atmospheric lifetime are likely to be produced by the sublimation.

The sublimation of the ice matrix at temperatures below the T_e of NaCl will therefore result in disintegrated small particles unless the solution is concentrated highly enough (above 35 psu, i.e., the equivalent to sea water salinity) to yield interconnected sponge-like structures. Surprisingly, when such sizable particles are further dried and warmed to room temperature, a large number of sub-micron sized crystals will appear (Figure 3). The particular conditions under which the small crystals form will be examined in the future; here, we hypothesize their connection with a close-to-eutectic amount of water, crystal-bound hydration water, or the amorphous solid brine, whose existence in the ice matrix was already reported (Imrichova et al., 2019). We have no data on the

mechanical stability of the observed clusters of crystals; the clusters, however, can be expected to disintegrate under a mechanical stress, through, for example, physical collisions in strong winds.

The provided images show that the micrometric crystals largely develop from ices with very low salt concentrations. The snow salinity on Antarctic sea ice was found to range from less than 0.1 psu to more than 100 psu (Massom et al., 2001). Very high snow salinities are detected mainly on the surfaces of young sea ice, especially in FFs (Douglas et al., 2012) and at the basal part of the snowpack; conversely, very low salinities appear at the top layer of the snowpack on sea ice (Domine et al., 2004), inland and/or near the coast. Recent cruise data from the Weddell Sea, Antarctica, indicate a median salinity of 0.06 psu (mean 0.31 psu) in the top 10 cm of snow (Frey et al., 2020). The lowest concentration applied in our study (0.085 psu) can therefore represent well the salinity on the surface layer of sea ice. In polar winter-spring, due to the net radiation cooling effect, the temperature at the surface of the snowpack on sea ice is often minimal compared to the temperatures beneath. Thus, the most exposed exterior layers of the snowpack (the coldest ones and those with relatively low salt concentrations) supposedly embody the media that best sublime into a multitude of small salt particles.

Highly saline FFs, exhibiting a salinity of up to 120 psu (Douglas et al., 2012), were previously thought to be a direct source of SSAs (Rankin, 2002). FFs grow on the surface of newly formed, fresh sea ice under calm conditions, especially at very low temperatures (Kaleschke, 2004). The low temperatures may well be a confounding factor between the growth of FFs and the formation of SSAs; our study indicates that aerosol-sized salt particles are mostly formed at low temperatures ($<$NaCl T_e). Frost flowers and SSAs, however, do not need to be interrelated causally. Although FFs are an unlikely direct source of SSAs even at temperatures below the NaCl T_e, the wind-cropped needles of FFs may contaminate the adjacent snow and, subsequently, get diluted through dissolution. The diluted salts may nevertheless retain the ability to form small salt particles after further sublimation. In addition, even the residua of FFs generated after the sublimation could supply an efficient surface for heterogeneous reactions, including halogen reactivation (Yang et al., 2017).

It has to be borne in mind that the morphologies of both the frozen solution and the final residuum depend on the freezing procedure; here, only one particular embodiment of the process is presented (Bartels-Rausch et al., 2014; Domine et al., 2013; Ebner et al., 2016; Imrichova et al., 2019; Ondrušková et al., 2020). Moreover, the freezing rate, linked to the sample cooling conditions, can strongly influence the distribution of impurities within the sample (Heger et al., 2005; Hullar & Anastasio, 2016; Vetráková et al., 2017). The variability characterizing the outcomes of the freezing impedes posing firm boundaries on concentrations that are typical of particular behavior. Nevertheless, the microscopic analysis allowed us to estimate the number of particles emanating from a unit of volume of the frozen solution at specific conditions (Text S7 in Supporting Information S1, Table S3 and S4 in Supporting Information S1). For example, the estimated number densities of salt vary from a minimum of ~300 particles mm^{-3} under 3.5 psu at −30°C to a maximum of ~3,100 particle mm^{-3} under 0.085 psu at −16°C. Further, let us note that the results have distinct consequences for the snowpack and sea ice as opposed to the blowing snow. We propose that the former foster the following process: Below the T_e and at low salt concentrations, small particles are produced, while above the T_e large salt chunks arise. This dual behavior, however, ceases to apply in the blowing snow, due to the relatively small size ranging from several tens to a few hundreds of microns and the fixed amount of salts contained in the particles when they become airborne. The particles produced by blowing snow will be smaller than the surface ice-generated ones on the condition that the size limits apply (Yang et al., 2019). Thus, the experimental results directly describe the sea ice and metamorphosed salty snow that has aged for several weeks or months, depending on the temperature (Domine et al., 2003; Rosenthal et al., 2007). Nonetheless, the observed phase behavior should be valid in all salty ices alike.

The sublimation in a microscope differs from that in a natural environment, especially as regards the absolute pressure and orientation. Previously, the method of ice sintering at a high vacuum and a low temperature was applied to identify the natural ice and snow impurities (Blackford et al., 2007; Cullen & Baker, 2001). The metamorphic processes in natural snow (Domine et al., 2003) and lab samples (Vetráková, et al., 2019) were already characterized. Here, we employ higher temperatures and pressures (as to comparing the values, see (Krausko et al., 2014)) to observe the ice sublimation products. An ice sample in a microscope experiences an upper draft, whereas blowing snow sublimes equally from all the sides. Therefore, we expect the mechanism of ice sublimation, and its temperature-controlled phase dependence in particular, to be identical in a microscope and in nature; however, the sublimation rates may differ substantially, as they are convection-limited (Jambon-Puillet et al., 2018). Other aspects not included in the current study, and ones possibly important for the outcome of the

sublimation, comprise the presence of dust, particulate matter (Domine et al., 2003), and organic compounds (Kirpes et al., 2019) on the one hand, and the absence of water vapor condensation on the other.

5. Conclusions

Although the actual sublimation processes in nature are far more complex than those within the ESEM chamber, our laboratory data show clear evidence to support the assumption that SSAs can originate from sublimating saline sea ice, surface snow, and blowing snow. Interestingly, we established that both the temperature and the salt concentration are important in terms of determining the size and number density of a salt particle formed during the sublimation process; thus, these two parameters are relevant for the chemistry of polar boundary layers and climate. In particular, at least 75% of the particles formed were smaller than 12 μm in the 0.085 psu ice sublimed at both −16 and −40°C and in the 0.85 and 3.5 psu ices sublimed at −40°C. Higher salt concentrations and sublimation temperatures resulted in larger particles. At −16°C, above the eutectic temperature of $NaCl \cdot 2H_2O$, water ice is solid, whereas a freeze-concentrated solution remains mostly liquid, producing large salt crystals (>100 μm) through the evaporation of the solution. Thus, temperatures above the T_e of NaCl restrict the formation of SSAs in frozen solutions concentrated above 0.85 psu. At the concentrations of 0.85 and 3.5 psu, we observed the smallest particles, delivered by the sublimation at −40°C (IQR = 4–9 μm); at such a temperature, most of the sea salts are solid. Already at −30°C were the particles more sizable (IQR = 9–29 μm), suggesting that the veins are partly liquid and that the solutes can communicate and aggregate. Above 35 psu, the sublimation, regardless of the temperature, produces particles sized within hundreds of micrometers, implying an extensive interconnection of the vein network. Surprisingly, when these particles are further dried and warmed up to +20°C, a large number of submicrometric crystals appear. Fractionated salt was noticed via an elemental analysis. This study establishes that the number and size of the SSAs that form through the sublimation process depend on the temperature and salt concentrations; these factors have not been considered to date in chemical models as regards the production of SSAs and the release of reactive bromine.

Data Availability Statement

The micrographs can be downloaded from https://www.doi.org/10.17632/hzh7y84hys.2.

References

Abbatt, J. P. D., Thomas, J. L., Abrahamsson, K., Boxe, C., Granfors, A., Jones, A. E., et al. (2012). Halogen activation via interactions with environmental ice and snow in the polar lower troposphere and other regions. *Atmospheric Chemistry and Physics*, *12*(14), 6237–6271. https://doi.org/10.5194/acp-12-6237-2012

Adler, G., Koop, T., Haspel, C., Taraniuk, I., Moise, T., Koren, I., et al. (2013). Formation of highly porous aerosol particles by atmospheric freeze-drying in ice clouds. *Proceedings of the National Academy of Sciences*, *110*(51), 20414–20419. https://doi.org/10.1073/pnas.1317209110

Barnes, P. R. F., Mulvaney, R., Robinson, K., & Wolff, E. W. (2002). Observations of polar ice from the Holocene and the glacial period using the scanning electron microscope. *Annals of Glaciology*, *35*, 559–566. https://doi.org/10.3189/172756402781816735

Barrie, L. A., Bottenheim, J. W., Schnell, R. C., Crutzen, P. J., & Rasmussen, R. A. (1988). Ozone destruction and photochemical-reactions at polar sunrise in the lower Arctic atmosphere. *Nature*, *334*(6178), 138–141. https://doi.org/10.1038/334138a0

Bartels-Rausch, T., Jacobi, H. W., Kahan, T. F., Thomas, J. L., Thomson, E. S., Abbatt, J. P. D., et al. (2014). A review of air–ice chemical and physical interactions (AICI): Liquids, quasi-liquids, and solids in snow. *Atmospheric Chemistry and Physics*, *14*(3), 1587–1633. https://doi.org/10.5194/acp-14-1587-2014

Bertram, T. H., Cochran, R. E., Grassian, V. H., & Stone, E. A. (2018). Sea spray aerosol chemical composition: Elemental and molecular mimics for laboratory studies of heterogeneous and multiphase reactions. *Chemical Society Reviews*, *47*(7), 2374–2400. https://doi.org/10.1039/c7cs00008a

Blackford, J. R., Jeffree, C. E., Noake, D. F. J., & Marmo, B. A. (2007). Microstructural evolution in sintered ice particles containing NaCl observed by low-temperature scanning electron microscope. *Proceedings of the Institution of Mechanical Engineers - Part L: Journal of Materials: Design and Applications*, *221*(3), 151–156. https://doi.org/10.1243/14644207jmda134

Bognar, K., Zhao, X., Strong, K., Chang, R. Y.-W., Frieß, U., Hayes, P. L., et al. (2020). Measurements of tropospheric bromine monoxide over four halogen activation seasons in the Canadian high Arctic. *Journal of Geophysical Research: Atmospheres*, *125*(18), e2020JD033015. https://doi.org/10.1029/2020JD033015

Bottenheim, J. W., Netcheva, S., Morin, S., & Nghiem, S. V. (2009). Ozone in the boundary layer air over the Arctic Ocean: Measurements during the TARA transpolar drift 2006–2008. *Atmospheric Chemistry and Physics*, *9*(14), 4545–4557. https://doi.org/10.5194/acp-9-4545-2009

Brady, J. B. (2009). Magma in a beaker: Analog experiments with water and various salts or sugar for teaching igneous petrology. *The Canadian Mineralogist*, *47*(2), 457–471. https://doi.org/10.3749/canmin.47.2.457

Chen, S., & Baker, I. (2010). Observations of the morphology and sublimation-induced changes in uncoated snow using scanning electron microscopy. *Hydrological Processes*, *24*(14), 2041. https://doi.org/10.1002/hyp.7689

Cullen, D., & Baker, I. (2001). Observation of impurities in ice. *Microscopy Research and Technique*, *55*(3), 198–207. https://doi.org/10.1002/jemt.10000

DeMott, P. J., Hill, T. C., McCluskey, C. S., Prather, K. A., Collins, D. B., Sullivan, R. C., et al. (2016). Sea spray aerosol as a unique source of ice nucleating particles. *Proceedings of the National Academy of Sciences*, *113*(21), 5797–5803. https://doi.org/10.1073/pnas.1514034112

Domine, F., Bock, J., Voisin, D., & Donaldson, D. J. (2013). Can we model snow photochemistry? Problems with the current approaches. *Journal of Physical Chemistry A*, *117*(23), 4733–4749. https://doi.org/10.1021/jp3123314

Domine, F., Lauzier, T., Cabanes, A., Legagneux, L., Kuhs, W. F., Techmer, K., & Heinrichs, T. (2003). Snow metamorphism as revealed by scanning electron microscopy. *Microscopy Research and Technique*, *62*(1), 33–48. https://doi.org/10.1002/jemt.10384

Domine, F., Sparapani, R., Ianniello, A., & Beine, H. J. (2004). The origin of sea salt in snow on Arctic sea ice and in coastal regions. *Atmospheric Chemistry and Physics*, *4*, 2259–2271. https://doi.org/10.5194/acp-4-2259-2004

Douglas, T. A., Domine, F., Barret, M., Anastasio, C., Beine, H. J., Bottenheim, J., et al. (2012). Frost flowers growing in the Arctic ocean-atmosphere–sea ice–snow interface: 1. Chemical composition. *Journal of Geophysical Research*, *117*. https://doi.org/10.1029/2011jd016460

Ebner, P. P., Schneebeli, M., & Steinfeld, A. (2016). Metamorphism during temperature gradient with undersaturated advective airflow in a snow sample. *The Cryosphere*, *10*(2), 791–797. https://doi.org/10.5194/tc-10-791-2016

Frey, M. M., Norris, S. J., Brooks, I. M., Anderson, P. S., Nishimura, K., Yang, X., et al. (2020). First direct observation of sea salt aerosol production from blowing snow above sea ice. *Atmospheric Chemistry and Physics*, *20*(4), 2549–2578. https://doi.org/10.5194/acp-20-2549-2020

Halfacre, J. W., Knepp, T. N., Shepson, P. B., Thompson, C. R., Pratt, K. A., Li, B., et al. (2014). Temporal and spatial characteristics of ozone depletion events from measurements in the Arctic. *Atmospheric Chemistry and Physics*, *14*(10), 4875–4894. https://doi.org/10.5194/acp-14-4875-2014

Hara, K., Osada, K., Kido, M., Hayashi, M., Matsunaga, K., Iwasaka, Y., et al. (2004). Chemistry of sea-salt particles and inorganic halogen species in Antarctic regions: Compositional differences between coastal and inland stations. *Journal of Geophysical Research: Atmospheres*, *109*(D20). https://doi.org/10.1029/2004jd004713

Hara, K., Osada, K., Yabuki, M., Takashima, H., Theys, N., & Yamanouchi, T. (2018). Important contributions of sea-salt aerosols to atmospheric bromine cycle in the Antarctic coasts. *Scientific Reports*, *8*(1), 13852. https://doi.org/10.1038/s41598-018-32287-4

Heger, D., Jirkovsky, J., & Klan, P. (2005). Aggregation of methylene blue in frozen aqueous solutions studied by absorption spectroscopy. *Journal of Physical Chemistry A*, *109*(30), 6702–6709. https://doi.org/10.1021/jp050439j

Hullar, T., & Anastasio, C. (2016). Direct visualization of solute locations in laboratory ice samples. *The Cryosphere*, *10*(5), 2057–2068. https://doi.org/10.5194/tc-10-2057-2016

Imrichova, K., Vesely, L., Gasser, T. M., Loerting, T., Nedela, V., & Heger, D. (2019). Vitrification and increase of basicity in between ice I_h crystals in rapidly frozen dilute NaCl aqueous solutions. *The Journal of Chemical Physics*, *151*(1), 014503. https://doi.org/10.1063/1.5100852

Jambon-Puillet, E., Shahidzadeh, N., & Bonn, D. (2018). Singular sublimation of ice and snow crystals. *Nature Communications*, *9*(1), 4191. https://doi.org/10.1038/s41467-018-06689-x

Kaleschke, L. (2004). Frost flowers on sea ice as a source of sea salt and their influence on tropospheric halogen chemistry. *Geophysical Research Letters*, *31*(16). https://doi.org/10.1029/2004gl020655

Keene, W. C., Maring, H., Maben, J. R., Kieber, D. J., Pszenny, A. A. P., Dahl, E. E., et al. (2007). Chemical and physical characteristics of nascent aerosols produced by bursting bubbles at a model air-sea interface. *Journal of Geophysical Research*, *112*(D21). https://doi.org/10.1029/2007jd008464

Killawee, J. A., Fairchild, I. J., Tison, J. L., Janssens, L., & Lorrain, R. (1998). Segregation of solutes and gases in experimental freezing of dilute solutions: Implications for natural glacial systems. *Geochimica et Cosmochimica Acta*, *62*(23/24), 3637–3655. https://doi.org/10.1016/S0016-7037(98)00268-3

Kirpes, R. M., Bonanno, D., May, N. W., Fraund, M., Barget, A. J., Moffet, R. C., et al. (2019). Wintertime Arctic sea spray aerosol composition controlled by sea ice lead microbiology. *ACS Central Science*, *5*(11), 1760–1767. https://doi.org/10.1021/acscentsci.9b00541

Krausko, J., Runštuk, J., Neděla, V., Klán, P., & Heger, D. (2014). Observation of a brine layer on an ice surface with an environmental scanning electron microscope at higher pressures and temperatures. *Langmuir*, *30*(19), 5441–5447. https://doi.org/10.1021/la500334e

Leck, C., Norman, M., Bigg, E. K., & Hillamo, R. (2002). Chemical composition and sources of the high Arctic aerosol relevant for cloud formation. *Journal of Geophysical Research*, *107*(D12). https://doi.org/10.1029/2001jd001463

Li, L., & Pomeroy, J. W. (1997). Probability of occurrence of blowing snow. *Journal of Geophysical Research*, *102*(D18), 21955–21964. https://doi.org/10.1029/97jd01522

Light, B., Brandt, R. E., & Warren, S. G. (2009). Hydrohalite in cold sea ice: Laboratory observations of single crystals, surface accumulations, and migration rates under a temperature gradient, with application to "Snowball Earth". *Journal of Geophysical Research*, *114*(C7). https://doi.org/10.1029/2008jc005211

Light, B., Maykut, G. A., & Grenfell, T. C. (2003). Effects of temperature on the microstructure of first-year Arctic sea ice. *Journal of Geophysical Research*, *108*(C2), 3051. https://doi.org/10.1029/2001jc000887

Marion, G. M., Farren, R. E., & Komrowski, A. J. (1999). Alternative pathways for seawater freezing. *Cold Regions Science and Technology*, *29*(3), 259–266. https://doi.org/10.1016/S0165-232X(99)00033-6

Massom, R. A., Eicken, H., Hass, C., Jeffries, M. O., Drinkwater, M. R., Sturm, M., et al. (2001). Snow on Antarctic sea ice. *Reviews of Geophysics*, *39*(3), 413–445. https://doi.org/10.1029/2000rg000085

May, N. W., Quinn, P. K., McNamara, S. M., & Pratt, K. A. (2016). Multiyear study of the dependence of sea salt aerosol on wind speed and sea ice conditions in the coastal Arctic. *Journal of Geophysical Research: Atmospheres*, *121*(15), 9208–9219. https://doi.org/10.1002/2016jd025273

Mulvaney, R., Wolff, E. W., & Oates, K. (1988). Sulfuric-acid at grain-boundaries in Antarctic ice. *Nature*, *331*(6153), 247–249. https://doi.org/10.1038/331247a0

Murphy, D. M., Anderson, J. R., Quinn, P. K., McInnes, L. M., Brechtel, F. J., Kreidenweis, S. M., et al. (1998). Influence of sea-salt on aerosol radiative properties in the Southern Ocean marine boundary layer. *Nature*, *392*(6671), 62–65. https://doi.org/10.1038/32138

Murray, B. J., Carslaw, K. S., & Field, P. R. (2021). Opinion: Cloud-phase climate feedback and the importance of ice-nucleating particles. *Atmospheric Chemistry and Physics*, *21*(2), 665–679. https://doi.org/10.5194/acp-21-665-2021

Nedela, V. (2007). Methods for additive hydration allowing observation of fully hydrated state of wet samples in environmental SEM. *Microscopy Research and Technique*, *70*(2), 95–100. https://doi.org/10.1002/jemt.20390

Neděla, V., Konvalina, I., Oral, M., & Hudec, J. (2015). The simulation of energy distribution of electrons detected by segmental ionization detector in high pressure conditions of ESEM. *Microscopy and Microanalysis*, *21*(S4), 264–269. https://doi.org/10.1017/S1431927615013483

Neděla, V., Tihlaříková, E., Runštuk, J., & Hudec, J. (2018). High-efficiency detector of secondary and backscattered electrons for low-dose imaging in the ESEM. *Ultramicroscopy*, *184*, 1–11. https://doi.org/10.1016/j.ultramic.2017.08.003

Neubauer, D., Ferrachat, S., Siegenthaler-Le Drian, C., Stier, P., Partridge, D. G., Tegen, I., et al. (2019). The global aerosol–climate model ECHAM6.3–HAM2.3—Part 2: Cloud evaluation, aerosol radiative forcing, and climate sensitivity. *Geoscientific Model Development*, *12*(8), 3609–3639. https://doi.org/10.5194/gmd-12-3609-2019

Nilsson, E. D., Rannik, Ü., Swietlicki, E., Leck, C., Aalto, P. P., Zhou, J., & Norman, M. (2001). Turbulent aerosol fluxes over the Arctic Ocean: 2. Wind-driven sources from the sea. *Journal of Geophysical Research*, *106*(D23), 32139–32154. https://doi.org/10.1029/2000jd900747

O'Dowd, C. D., Smith, M. H., Consterdine, I. E., & Lowe, J. A. (1997). Marine aerosol, sea-salt, and the marine sulphur cycle: A short review. *Atmospheric Environment*, *31*(1), 73–80. https://doi.org/10.1016/S1352-2310(96)00106-9

Ohno, H., Igarashi, M., & Hondoh, T. (2005). Salt inclusions in polar ice core: Location and chemical form of water-soluble impurities. *Earth and Planetary Science Letters*, *232*(1–2), 171–178. https://doi.org/10.1016/j.epsl.2005.01.001

Ondrušková, G., Veselý, L., Zezula, J., Bachler, J., Loerting, T., & Heger, D. (2020). Using Excimeric Fluorescence to Study How the Cooling Rate Determines the Behavior of Naphthalenes in Freeze-Concentrated Solutions: Vitrification and Crystallization. *The Journal of Physical Chemistry B*, *124*(46), 10556–10566. https://doi.org/10.1021/acs.jpcb.0c07817

Oyabu, I., Iizuka, Y., Kawamura, K., Wolff, E., Severi, M., Ohgaito, R., et al. (2020). Compositions of dust and sea salts in the Dome C and Dome Fuji ice cores from Last Glacial Maximum to early Holocene based on ice-sublimation and single-particle measurements. *Journal of Geophysical Research: Atmospheres*, *125*(4). https://doi.org/10.1029/2019jd032208

Patterson, J. P., Collins, D. B., Michaud, J. M., Axson, J. L., Sultana, C. M., Moser, T., et al. (2016). Sea spray aerosol structure and composition using cryogenic transmission electron microscopy. *ACS Central Science*, *2*(1), 40–47. https://doi.org/10.1021/acscentsci.5b00344

Pohler, D., Vogel, L., Friess, U., & Platt, U. (2010). Observation of halogen species in the Amundsen Gulf, Arctic, by active long-path differential optical absorption spectroscopy. *Proceedings of the National Academy of Sciences*, *107*(15), 6582–6587. https://doi.org/10.1073/pnas.0912231107

Rankin, A. M., Wolff, E. W., & Martin, S. (2002). Frost flowers: Implications for tropospheric chemistry and ice core interpretation. *Journal of Geophysical Research*, *107*(D23), 4–1. https://doi.org/10.1029/2002jd002492

Rhodes, R. H., Yang, X., Wolff, E. W., McConnell, J. R., & Frey, M. M. (2017). Sea ice as a source of sea salt aerosol to Greenland ice cores: A model-based study. *Atmospheric Chemistry and Physics*, *17*(15), 9417–9433. https://doi.org/10.5194/acp-17-9417-2017

Roscoe, H. K., Brooks, B., Jackson, A. V., Smith, M. H., Walker, S. J., Obbard, R. W., & Wolff, E. W. (2011). Frost flowers in the laboratory: Growth, characteristics, aerosol, and the underlying sea ice. *Journal of Geophysical Research*, *116*(D12). https://doi.org/10.1029/2010jd015144

Rosenthal, W., Saleta, J., & Dozier, J. (2007). Scanning electron microscopy of impurity structures in snow. *Cold Regions Science and Technology*, *47*(1–2), 80–89. https://doi.org/10.1016/j.coldregions.2006.08.006

Sakurai, T., Iizuka, Y., Horikawa, S., Johnsen, S., Dahl-Jensen, D., Steffensen, J. P., & Hondoh, T. (2009). Direct observation of salts as micro-inclusions in the Greenland GRIP ice core. *Journal of Glaciology*, *55*(193), 777–783. https://doi.org/10.3189/002214309790152483

Shepson, P. B. (2021). Cryosphere-Atmosphere Interactions. In *Chemistry in the cryosphere* (pp. 1–56).

Tarasick, D. W., & Bottenheim, J. W. (2002). Surface ozone depletion episodes in the Arctic and Antarctic from historical ozonesonde records. *Atmospheric Chemistry and Physics*, *2*(3), 197–205. https://doi.org/10.5194/acp-2-197-2002

Vetráková, Ľ., Neděla, V., Runštuk, J., & Heger, D. (2019). The morphology of ice and liquid brine in an environmental scanning electron microscope: A study of the freezing methods. *The Cryosphere*, *13*(9), 2385–2405. https://doi.org/10.5194/tc-13-2385-2019

Vetráková, Ľ., Neděla, V., Runštuk, J., Tihlaříková, E., Heger, D., & Shalaev, E. (2020). Dynamical in-situ observation of the lyophilization and vacuum-drying processes of a model biopharmaceutical system by an environmental scanning electron microscope. *International Journal of Pharmaceutics*, *585*, 119448. https://doi.org/10.1016/j.ijpharm.2020.119448

Vetráková, Ľ., Vykoukal, V., & Heger, D. (2017). Comparing the acidities of aqueous, frozen, and freeze-dried phosphate buffers: Is there a "pH memory" effect? *International Journal of Pharmaceutics*, *530*(1–2), 316–325. https://doi.org/10.1016/j.ijpharm.2017.08.005

Wagenbach, D., Ducroz, F., Mulvaney, R., Keck, L., Minikin, A., Legrand, M., et al. (1998). Sea-salt aerosol in coastal Antarctic regions. *Journal of Geophysical Research*, *103*(D9), 10961–10974. https://doi.org/10.1029/97jd01804

Wilson, T. W., Ladino, L. A., Alpert, P. A., Breckels, M. N., Brooks, I. M., Browse, J., et al. (2015). A marine biogenic source of atmospheric ice-nucleating particles. *Nature*, *525*(7568), 234–238. https://doi.org/10.1038/nature14986

Wise, M. E., Baustian, K. J., Koop, T., Freedman, M. A., Jensen, E. J., & Tolbert, M. A. (2012). Depositional ice nucleation onto crystalline hydrated NaCl particles: A new mechanism for ice formation in the troposphere. *Atmospheric Chemistry and Physics*, *12*(2), 1121–1134. https://doi.org/10.5194/acp-12-1121-2012

Yang, X., Frey, M. M., Rhodes, R. H., Norris, S. J., Brooks, I. M., Anderson, P. S., et al. (2019). Sea salt aerosol production via sublimating wind-blown saline snow particles over sea ice: Parameterizations and relevant microphysical mechanisms. *Atmospheric Chemistry and Physics*, *19*(13), 8407–8424. https://doi.org/10.5194/acp-19-8407-2019

Yang, X., Neděla, V., Runštuk, J., Ondrušková, G., Krausko, J., Vetráková, Ľ., & Heger, D. (2017). Evaporating brine from frost flowers with electron microscopy and implications for atmospheric chemistry and sea-salt aerosol formation. *Atmospheric Chemistry and Physics*, *17*(10), 6291–6303. https://doi.org/10.5194/acp-17-6291-2017

Yang, X., Pyle, J. A., & Cox, R. A. (2008). Sea salt aerosol production and bromine release: Role of snow on sea ice. *Geophysical Research Letters*, *35*(16). https://doi.org/10.1029/2008gl034536